Dipalmitoyl-phosphatidylserine-filled cationic maltodextrin nanoparticles exhibit enhanced efficacy for cell entry and intracellular protein delivery in phagocytic THP-1 cells.

Clément Brinkhuizen, Damien Shapman, A. Lebon, M. Bénard, Meryem Tardivel, Laurent Dubuquoy, L. Galas, Rodolphe Carpentier

Research Article

Clément Brinkhuizen, Damien Shapman, Alexis Lebon, Magalie Bénard, Meryem Tardivel, Laurent Dubuquoy, Ludovic Galas, Rodolphe Carpentier*

Dipalmitoyl-phosphatidylserine-filled cationic maltodextrin nanoparticles exhibit enhanced efficacy for cell entry and intracellular protein delivery in phagocytic THP-1 cells

https://doi.org/10.1515/bmc-2022-0029
received March 29, 2023; accepted May 8, 2023

Abstract: Vaccination through the upper respiratory tract is a promising strategy, and particulate antigens, such as antigens associated with nanoparticles, triggered a stronger immune response than the sole antigens. Cationic maltodextrin-based nanoparticles loaded with phosphatidylglycerol (NPPG) are efficient for intranasal vaccination but non-specific to trigger immune cells. Here we focused on phosphatidylserine (PS) receptors, specifically expressed by immune cells including macrophages, to improve nanoparticle targeting through an efferocytosis-like mechanism. Consequently, the lipids associated with NPPG have been substituted by PS to generate cationic maltodextrin-based nanoparticles with dipalmitoyl-phosphatidylserine (NPPS). Both NPPS and NPPG exhibited similar physical characteristics and intracellular distribution in THP-1 macrophages. NPPS cell entry was faster and higher (two times more) than NPPG. Surprisingly, competition of PS receptors with phospho-L-serine did not alter NPPS cell entry and annexin V did not preferentially interact with NPPS. Although the protein association is similar, NPPS delivered more proteins than NPPG in cells. On the contrary, the proportion of mobile nanoparticles (50%), the movement speed of nanoparticles (3 µm/5 min), and protein degradation kinetics in THP-1 were not affected by lipid substitution. Together, the results indicate that NPPS enter cells and deliver protein better than NPPG, suggesting that modification of the lipids of cationic maltodextrin-based nanoparticles may be a useful strategy to enhance nanoparticle efficacy for mucosal vaccination.

Keywords: nanoparticle, vaccine, phospholipids, efferocytosis, targeting

Abbreviations

DPPS	dipalmitoyl-phosphatidylserine
NP^+	Cationic maltodextrin-based nanoparticles
NPPS	NP^+ with DPPS
NPPG	NP^+ with dipalmitoyl-phosphatidylglycerol
PS	phosphatidylserine
L-pSer	phospho-L-serine

Introduction

Intranasal vaccination is an interesting alternative strategy to intramuscular administration because it better mimics infection at the mucosal surfaces through which most of the pathogens enter the body [1]. However, the lack of effective mucosal adjuvant, mucosal enhancer, or mucosal immune booster may limit the efficacy of vaccine through upper respiratory tract. In this regard, nanocarriers, which are able to associate with, protect, and deliver antigens through the mucosal barrier, are promising [2,3]. Since cationic maltodextrin-based nanoparticles (NP^+) have been successfully used through intranasal instillation, they are now considered as mucosal enhancer of antigenic protein

* **Corresponding author: Rodolphe Carpentier**, University Lille, Inserm, CHU Lille, U1286 - INFINITE – Institute for Translational Research in Inflammation, F-59000 Lille, France,
e-mail: rodolphe.carpentier@univ-lille.fr
Clément Brinkhuizen, **Laurent Dubuquoy:** University Lille, Inserm, CHU Lille, U1286 - INFINITE – Institute for Translational Research in Inflammation, F-59000 Lille, France
Damien Shapman, **Alexis Lebon**, **Magalie Bénard**, **Ludovic Galas:** University of Rouen Normandy, INSERM US 51, CNRS UAR 2026, HeRacLeS-PRIMACEN, Normandie Université, 76000 Rouen, France
Meryem Tardivel: University Lille, CNRS, Inserm, CHU Lille, Institut Pasteur de Lille, US 41 - UAR 2014 - PLBS, F-59000 Lille, France

delivery [4]. As a result of the synthesis process, NP^+ are porous nanoparticles with a homogeneous cationic charge distribution along the maltodextrin matrix. When anionic phospholipids such as dipalmitoyl-phosphatidylglycerol (DPPG) are loaded to NP^+, NPPGs (formerly called NPL, DGNP, or DG70) with higher molecular weight and similar size and zeta potential [5,6] are generated, proving that lipids are not associated with the nanoparticles' surface. Furthermore, NPPGs show weaker interactions with mucus than NP^+, suggesting that the lipids associated with the NP^+ matrix can interact with the surrounding mucins [7]. In another experiment, proteins associated with NPPG did not decrease the zeta potential and continued to be accessible by biological compounds like enzymes [5,6]. This suggests that the porous nature of NP^+ and NPPG allows interactions of the surrounding environment with the core of the particles, either the matrix or the associated lipids.

NPPGs were able to associate and deliver a wide variety of proteins into epithelia [6,8–10] and trigger an immune response when associated with antigens and administered into nasal cavity [9,11,12]. Nevertheless, the detailed mechanism from antigen delivery to the nanoparticle-assisted immune response remains a matter of debate. Previous works have shown that NPPGs increase the nasal residence time of associated antigens [13], but do not cross the nasal epithelial barrier as they were being collected by the mucociliary system and eliminated through the digestive tract [8,14]. However, these studies focused mainly on epithelial cells, while immune cells should be considered, as demonstrated by the interaction between NPPG and immune cells, including macrophages and dendritic cells *in vitro* [10,13] or splenocytes *ex vivo* [9,15].

Phosphatidylserine (PS) is a *eat-me* signal allowing phagocytes to engulf apoptotic cells in a process called efferocytosis [16]. In addition, macrophages exhibited a large diversity of membrane receptors involved in efferocytosis presenting an affinity for PS. In particular, four members of T-cell immunoglobulin and mucin domain (TIM) receptor family that directly bind with PS [17] are expressed by epithelial macrophages [18,19]. Within the Tyro3-Axl-Mer (TAM) tyrosine kinase receptor family, Axl and Mer also have affinity for PS and have been detected in macrophages [20]. Other receptors, including brain-specific angiogenesis inhibitor 1, CD300, PS receptor (PSR) (JMJD6), or receptor for advanced glycosylation end products, are likewise proposed receptors for PS-mediated efferocytosis [20]. Alternatively, PS receptors may also be hijacked by viruses [21,22] and parasites [23,24] to enter cells or evade from immune vigilance. PS may consequently represent a prime target for immune cells and more specifically for phagocytic antigen-presenting cells that can also be strategically used for NP^+ that behave like synthetic viruses or parasites [12,14].

Since lipids associated with the NP^+ core could interact with the surrounding environment [5–7], we thus hypothesise that substituting DPPG in NPPG by dipalmitoyl-phosphatidylserine (DPPS), leading to the formation of NPPS, could target the nanoparticles to PS receptor-expressing cells like macrophages. As a model to investigate the mechanism of nanoparticle-immune cell interactions, we used macrophage-like THP-1 cells, a well-described monocyte cell line that can easily differentiate into macrophages expressing numerous PS receptors [25]. Consequently, after validating that macrophage-like THP-1 cells were competent for efferocytosis, we compared the ability of NPPG vs NPPS to enter, associate with, and deliver proteins in these cells. Finally, we also characterised nanoparticle intracellular routes and processing through cell imaging and flow cytometry analyses.

Material and methods

Synthesis, labelling and lipidation of nanoparticles

The nanoparticles were synthesised as described previously [26]. The maltodextrin (Glucidex 6, Roquette, France) was dissolved in a Eq/L sodium hydroxide solution with magnetic stirring at room temperature, then epichlorohydrin and glycidyl trimethyl ammonium chloride (Sigma-Aldrich, France) were added, leading to the formation of a cationic hydrogel. The gel was then neutralised with acetic acid and crushed by a high-pressure homogeniser (LM20-30 microfluidizer, Microfluidics, France). The nanoparticles were purified from oligosaccharides, low-molecular weight reagents, and salts by tangential flow ultra-filtration (Akta Flux6, GE Healthcare, France) using a 300 kDa cut-off hollow fiber. The resulting purified cationic particles, called NP^+, were the common intermediate for obtaining NPPG and NPPS. NPPGs are cationic and porous nanoparticles loaded with 1,2-dipalmitoyl-sn-glycero-3-PG (DPPG, Bertin bioreagent, France) while NPPS are loaded with 1,2-dipalmitoyl-sn-glycero-3-PS (DPPS, Bertin bioreagent, France). Whenever necessary, NP^+ were labelled by fluorescein isothiocyanate (FITC, Thermo Fisher Scientific, France) according to Dombu et al. [5]. In a 0.1 M bicarbonate buffer with pH = 8.3, NP^+ were labelled by 1% (w:w) of FITC for 12 h. Labelled NP^+ were further purified by gel permeation chromatography on a PD-10 Sephadex desalting column (Sigma Aldrich,

France). NP^+ (or NP^+-FITC) was loaded with 70% (w:w) of phospholipids (DPPG or DPPS) as previously described [26]. Phospholipids were dissolved in a 17% (w:v) aqueous solution of solutol HS15 (Sigma Aldrich, France), then mixed at 80°C with nanoparticles until complete incorporation. The resulting NPPGs or NPPSs were filtered through 0.2 µm polyethersulfone membrane.

Characterization of nanoparticles

The size and zeta potential of the nanoparticles were determined as previously described [26]. The hydrodynamic diameter (number) of the nanoparticles was measured by dynamic light scattering (Zetasizer nano ZS, Malvern UK) at 25°C, using 1 mg/mL nanoparticles in an aqueous solution of 15 mM NaCl. The zeta potential of the nanoparticles was measured by electrophoretic light scattering (Zetasizer nano ZS) at 25°C, using nanoparticles at 1 mg/mL in ultrapure water.

Cell culture

THP-1 cell (ATCC #TIB-202) is a monocyte isolated from peripheral blood from an acute monocytic leukaemia patient. Mycoplasma-free cells were maintained in Roswell Park Memorial Institute-1640 (RPMI-1640; Thermo Fisher Scientific) medium supplemented with 2 mM of L-glutamine, 10% heat-inactivated fetal bovine serum, 100 U/mL penicillin, and 100 µg/mL streptomycin (Thermo Fisher Scientific). Cells were incubated at 37°C in a humidified atmosphere with 5% CO_2. For cytometry analyses, THP-1 cells were seeded at a density of 2.0×10^5 cells per well (1.9 cm^2) in 24-well plates. For live-cell imaging, THP-1 cells were plated at a density of 0.4×10^4 cells per cm^2 on 35 mm glass bottom microwell dishes (MatTek Corporation, Ashland, MA, USA). The cells were then differentiated into macrophages (macrophage-like THP-1 cells) with 40 ng/mL of phorbol 12-myristate 13-acetate (PMA, Sigma-Aldrich, France) for 48 h followed by a recovery period of 24 h without PMA.

Efferocytosis assay

The ability of macrophage-like THP-1 cells to phagocytose apoptotic cells was assessed using the Efferocytosis assay kit (Bertin bioreagent, France) according to the manufacturer's instructions. Jurkat cells, an immortalised line of human T lymphocyte, were used as bait and were cultured using the same conditions as THP-1 cells. Briefly, THP-1 cells were labelled with CytoTell Blue™ and differentiated into macrophages. Then, Jurkat cells were labelled with carboxyfluorescein succinimidyl ester (CFSE) and treated with staurosporine for 6 h to induce apoptosis. Afterwards, apoptotic Jurkat cells were co-cultured for 18 h with macrophage-like THP-1 cells (cellular ratio 1:1) and cells were collected for flow cytometry analysis (Attune NxT, Thermo Fisher Scientific, France). A minimum of 5,000 cells were first selected based on their size and internal complexity (FSC/SSC), then the fluorescence intensities related to the cellular labels were determined using the following excitation/emission wavelengths (nm): CytoTell Blue: 405/450, CFSE: 488/525.

Confocal microscopy

An inverted confocal laser scanning microscope (STELLARIS 8, Leica Microsystems, Nanterre, France) equipped with a white light laser (440–790 nm), an 86X objective (NA = 1.20, water immersion, WD = 300 µm) were used in this study. Fluorescence signal was detected (500–550 nm) in photon counting mode through new generation Power HyD detectors (Power HyD-S, Silicon Multi-Pixel Photon Counter). Confocal imaging of nanoparticle-labelled living macrophage-like THP-1 cells was performed with 488 nm WLL line (2% AOTF) for FITC excitation. A full bold line Okolab chamber (Ottaviano, Italy) installed on the inverted microscope stand was used to keep the temperature at 37°C during image acquisition. *Z*-stack was obtained at a step of 300 nm with a total thickness of 14.1 µm. Bright-field image was acquired through activation of transmitted light detector. Images were processed through ImageJ for maximum projection and overlay.

TIRF microscopy

For live-cell imaging, macrophage-like THP-1 cells were exposed to 5 µg/mL of NPPS or NPPG for 0.5 or 2 h in RPMI-1640 medium. Afterward, cells were washed three times with the medium for 2 min each and kept in culture medium for observation. Total internal reflection fluorescence (TIRF) imaging (Leica Microsystems) of nanoparticle-internalised living macrophage-like THP-1 cells was performed with 488 nm line (25% AOTF) for FITC excitation and sCMOS camera (Hamamatsu, Massy, France) for fluorescence

collection through 100× (NA = 1.46, oil immersion, WD = 0.17 µm) objective and GFP filter (excitation/bandwidth: 475/40 nm; dichroic cut: 495 nm; emission/bandwidth: 530/50 nm). TIRF microscopy was performed with a depth penetration of 150 nm and a single focus plane was acquired. Time-lapse was obtained at a frequency of one image every 2 s during 5 min. A full bold line Okolab chamber (PeCon, Erbach, Germany) installed on the inverted microscope stand was used to keep the temperature at 37°C during image acquisition. Images were processed through ImageJ for contrast adjustment and through Imaris (version 9.0.2, Oxford Instruments, Zurich, Switzerland) for nanoparticle counting and tracking. In particular, nanoparticles were automatically detected as single spherical spots through application of segmentation algorithm and thresholding to fluorescence signal while cell surface area was determined through a cell mask. Consequently, densities of nanoparticles were obtained as a ratio of nanoparticle number to cell surface (mm^2).

Determination of nanoparticles cell entry by flow cytometry

Macrophage-like THP-1 cells were exposed to 10 µg/mL of FITC-labelled nanoparticles for 0.5, 1, 2, 4, or 6 h and collected using trypsin before flow cytometry analysis (Attune NxT, Thermo Fisher Scientific, France) using the following excitation/emission wavelengths (nm): FITC: 488/525. A minimum of 5,000 cells were first selected according to their size and internal complexity (FSC/SSC), then the fluorescence intensity related to the cellular content was determined. To compete with the PS receptors, cells were pretreated for 30 min with 2 mM phospho-L-serine (L-pSer) as previously described [27].

DPPS accessibility

To assess the accessibility of DPPS from the surrounding environment of the NPPS, annexin V, a PS binding protein, was used. FITC-labelled nanoparticles (5 µg) was mixed with 0.25, 1.25, or 2.5 µg of annexin V-AF647 (640943, Biolegend, France) in a calcium-containing buffer (10 mM HEPES, 140 mM NaCl, 2.5 mM $CaCl_2$, pH = 7.4) for 30 min at room temperature. The binding of annexin V to the nanoparticles was evaluated by flow cytometry (CytoFlex, Beckman Coulter, France). A minimum of 450,000 nanoparticles were first selected with FITC fluorescence intensity (excitation/emission (bandwidth) wavelengths: 488 nm/525(40) nm) in comparison with the unlabelled nanoparticles. The annexin V-AF647 (excitation/emission (bandwidth) wavelengths: 638 nm/660(10) nm) was analysed in the FITC positive nanoparticle region.

Association of proteins with nanoparticles

Bovine serum albumin (BSA, Sigma Aldrich, France) was used as a model protein. The loading of BSA in nanoparticles was performed by mixing both components in an aqueous solution at room temperature for 1 h. Different ratios (w:w) of nanoparticles/BSA were used from 1/0 to 1/5. The size and zeta potential were determined as described for the characterisation of the nanoparticles. The association of BSA with the nanoparticles was analysed by non-denaturing PAGE as previously described [10]. Gels were scanned and quantified using the ImageJ software, setting the 0% of association over the BSA alone input while 100% of association was set to the blank protein lane (NPPS or NPPG alone).

Intracellular delivery of proteins

BSA labelled with FITC (BSA-FITC, Sigma Aldrich, France) was associated with nanoparticles at a ratio (w:w) nanoparticle/protein of 3/1. Then, macrophage-like THP-1 cells were exposed to 10 µg/mL of the formulations for 0.5, 1, 2, 4 or 6 h and collected using trypsin before flow cytometry analysis (Attune NxT, Thermo Fisher Scientific) using the following excitation/emission wavelengths (nm): FITC: 488/525. A minimum of 5,000 cells were first selected according to their size and internal complexity (FSC/SSC) then the fluorescence intensity related to the BSA-FITC cellular content was determined.

Intracellular degradation of proteins

BSA-DQ (DQ™-green BSA, Sigma Aldrich, France) is a Bodipy-FL over-labelled protein used as a reporter of protein degradation. BSA-DQ was associated with nanoparticles at a nanoparticle/protein ratio (w:w) of 3/1. Then, macrophage-like THP-1 cells were exposed to 10 µg/mL of the formulations for 0.5, 1, 2, 4, or 6 h and collected using trypsin before flow cytometry analysis (Attune NxT, Thermo Fisher Scientific) using the following excitation/emission wavelengths (nm): 488/525. A minimum of 5,000 cells were first selected based on their size and internal complexity (FSC/SSC), then the

fluorescence intensity related to the cellular content of Bodipy-FL-labelled peptides released by the degradation of BSA-DQ was determined. To assess the involvement of acid endosomes (i.e. lysosomes) in the process of BSA degradation delivered by nanoparticles, macrophage-like THP-1 cells were pretreated for 15 min with 50 mM of chloroquine diphosphate salt (Thermo Fisher Scientific), then exposed for 30 min to the BSA-DQ formulations before flow cytometry analysis. For longer time of exposure, a pH-sensitive fluorophore was used. BSA was labelled with pHrodo (pHrodo™ Red, SE, Thermo Fisher Scientific) according to the manufacturer's instructions using 1% (w:w) of label. BSA-pHrodo was further purified by gel permeation chromatography on a PD-10 Sephadex desalting column (Sigma Aldrich, France) and the protein content was determined by the microBCA method (microBCA assay kit, Thermo Fisher Scientific). BSA-pHrodo was associated with nanoparticles at a nanoparticle/protein ratio (w:w) of 3/1. Then, macrophage-like THP-1 cells were exposed to 10 µg/mL of the formulations for 0.5, 1, 2, 4, or 6 h and collected using trypsin before flow cytometry analysis (Attune NxT, Thermo Fisher Scientific) using the following excitation/emission wavelengths (nm): 560/585. A minimum of 5,000 cells were first selected based on their size and internal complexity (FSC/SSC), then the fluorescence intensity related to the cellular content of low pH-activated BSA-pHrodo was determined.

Statistics

All experiments were done at least three times. The distribution of the quantitative variables was assessed by the Shapiro–Wilk test completed by the calculation of the residuals and the coefficients of Skewness and Kurtosis. Student's tests and ANOVA with Tukey-Kramer correction were used to compare quantitative values. For kinetic analyses, multivariate regression with repeated measurements was used. All tests were performed with a risk alpha of 5% using the SAS Software (version 9.04.01M6P11072018). Only statistically significant differences are indicated in the figures.

Results

Characterisation of the cationic maltodextrin nanoparticles and macrophage-like THP-1 cells

NPPSs and NPPGs are NP^+ containing DPPS and DPPG, respectively. To strictly compare the effect of lipids on cell entry and protein delivery, a common batch of NP^+ was used, which was filled with either DPPS or DPPG. The characterisation of nanoparticles using light scattering approaches revealed that NPPS and NPPG had similar (i) median hydrodynamic diameter (number size), (ii) interquartile range (from 0.178 to 0.269) of the polydispersity index (PDI), and (iii) zeta potential values (Table 1).

Since the polysaccharide matrix, the size, and the zeta potential of NPPS and NPPG were identical, the differential cellular effects could only be attributed to the associated lipid composition. The colloidal stability of nanoparticles was then determined weekly by measuring the size of the NPPS and NPPG stored in water at room temperature. No significant variations in the nanoparticle size could be detected during 28 weeks (Figure 1) demonstrating a robust colloidal stability of NPPS and NPPG over time in aqueous medium. Then, the ability of macrophage-like THP-1 cells to phagocyte apoptotic Jurkat cells via a PS-dependent efferocytosis mechanism was assessed through flow cytometry. Derived from monocytes, THP-1 cells were differentiated into macrophages after stimulation with PMA and labelled with CytoTell Blue. In parallel, immortalised human T lymphocyte Jurkat cells were labelled with CFSE and treated with staurosporine to induce apoptosis and exposure of the PS *eat me* signal on the outer plasma membrane. Both cell types were then co-cultured for 18 h and flow cytometry analyses revealed that more than 20% of Jurkat cells were engulfed by macrophage-like THP-1 cells (Figure 2). These data show that phagocytic macrophage-like THP-1 cells are competent for efferocytosis and expressed the relevant PS-receptors that can potentially be targeted by PS-containing nanoparticles.

Table 1: Size and zeta potential of NPPS and NPPG

	Number size (nm)	PDI	Zeta potential (mV)
NPPS	35.00 (30.00; 38.75)	0.195 (0.178; 0.269)	26 (26; 28)
NPPG	36.50 (25.50; 38.25)	0.254 (0.178; 0.261)	27 (26; 29)

Note: The median and interquartile of the hydrodynamic diameter (expressed as number size), polydispersity index (PDI), and zeta potential are indicated in the above table.

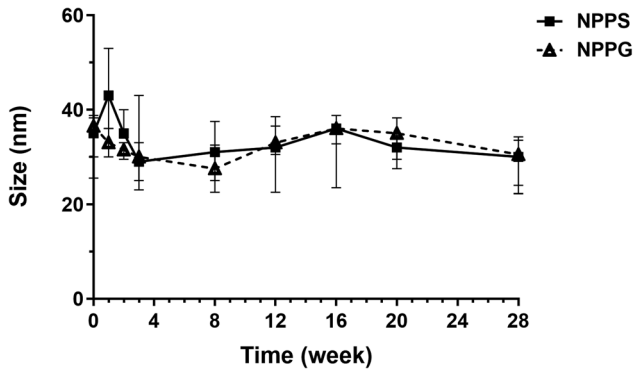

Figure 1: Colloidal stability of NPPS and NPPG. The nanoparticles are stored for 28 weeks at room temperature in water. The hydrodynamic diameter of NPPS and NPPG are monitored by dynamic light scattering after sterile sampling of the nanoparticles. The graph represents the median and the interquartile of at least 6 samples. No significant difference is observed between NPPS and NPPG.

Effect of associated lipid composition on cell entry efficacy

To study the impact of the lipid composition on the nanoparticle ability to penetrate macrophage-like THP-1 cells, two complementary strategies were used. Nanoparticle cell entry was first investigated in isolated living macrophage-like THP-1 cells with FITC-labelled NPPS and NPPG (5 µg/mL) through confocal and TIRF microscopies. On the cover glass, adherent macrophage-like THP-1 cells mainly showed rounded "fried egg"-like morphology with variable-sized basal lamellipodia (Figure 3a, white arrows). Confocal imaging revealed the presence of NPPS and NPPG in both lamellipodia and cytoplasm surrounding the nucleus (Figure 3a) suggesting that there is no specific site for nanoparticle entry in macrophage-like THP-1 cells. However, TIRF experiments indicated that NPPS and NPPG were mainly motionless in the lamellipodia in contrary to the upper cytoplasm. Consequently, for time resolution and standardisation purposes, images were only acquired at the cell body mid-plane and considered as a cell index for NPPS and NPPG TIRF evaluation. In this configuration, NPPS and NPPG were mainly distributed in the periphery of the cells after 0.5 h exposure and more widely found within the entire cytoplasm after 2 h of cell contact (Figure 3b and c). In particular, the density of NPPS and NPPG within the focus plan significantly increased over time of exposure (Figure 3d). In addition, NPPS density was slightly higher than NPPG (565 ± 47 vs 459 ± 45 particles/mm^2) after 0.5 h-exposure, suggesting that NPPS may have entered the macrophage-like THP-1 cells faster than NPPG. Then, nanoparticle cell entry was studied in living cell population through flow cytometry. In microplates, macrophage-like THP-1 cells were exposed to 10 µg/mL of FITC-labelled nanoparticles up to 6 h and the overall cellular content of fluorescent nanoparticles was detected. Macrophage-like THP-1 cells loaded with NPPG showed a constant increase (linear slope) in intracellular NPPG content from 0.5 to 6 h (Figure 4). In contrast, NPPS cell entry displayed a strong initial start within the first 2 h followed by a progressive increase during the next 4 h (Figure 4). Although NPPG and NPPS loading exhibited parallel increase in slope from 2 to 6 h, the NPPS intensity signal is about two times higher than NPPG one.

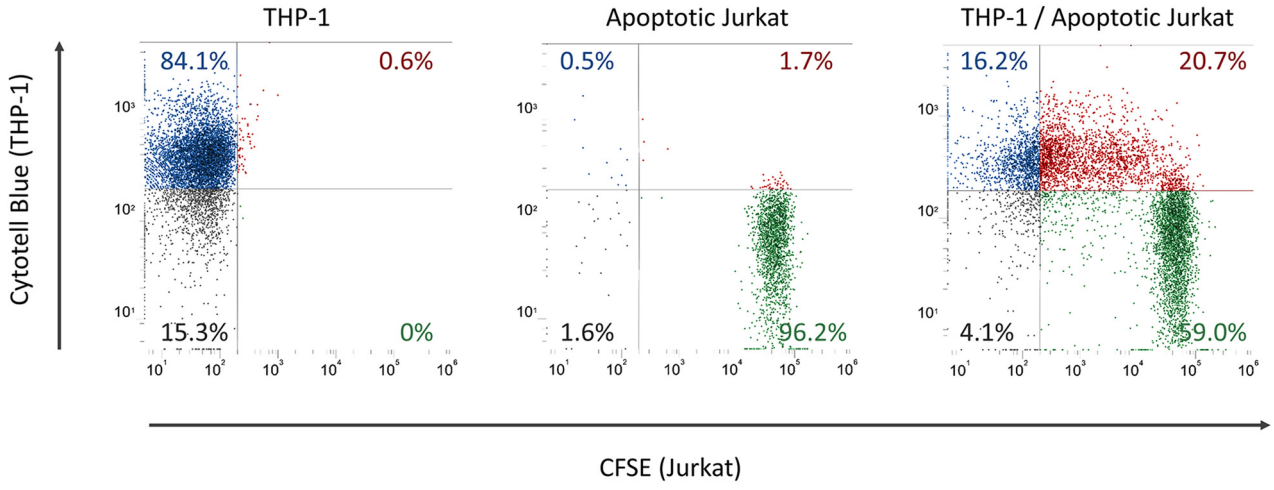

Figure 2: Macrophage-like THP-1 cells carry out efferocytosis. THP-1 are labelled with CytoTell Blue® (left) while apoptotic Jurkat cells are labelled with CFSE (middle) as revealed by cytometry. THP-1 are co-cultured with apoptotic Jurkat (ratio 1:1) for 18 h (right), then cytometry analyses show that more than 20% of THP-1 cells have done efferocytosis. Grey: unlabelled cells, blue: CytoTell Blue®-positive THP-1 cells, green: CFSE-positive Jurkat cells, red: CytoTell Blue®-CFSE double positive THP-1 cells having captured apoptotic Jurkat cells.

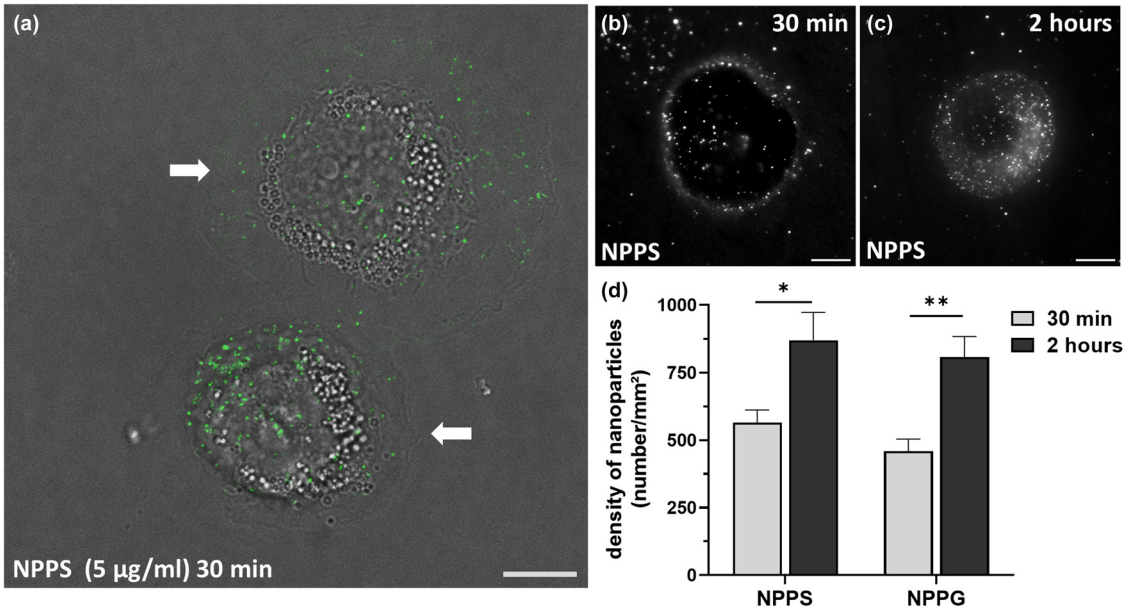

Figure 3: Internalised nanoparticle imaging in living macrophage-like THP-1 cells. (a) Macrophage-like THP-1 cells were exposed to 5 µg/mL of NPPS for 30 min and imaged by confocal microscopy (Green, FITC-labelled nanoparticles, maximum projection; Grey, bright field, white arrows indicated lamellipodia edges). Scale bar: 10 µm. (b and c) Macrophage-like THP-1 cells were exposed to 5 µg/mL of NPPS for 30 min (b) or 2 h (c) and imaged in a single focal plan at the mid-cell body level by TIRF microscopy. Scale bar: 10 µm. (d) Density of nanoparticles within a single focus plane of macrophage-like THP-1 cells through TIRF microscopy are represented as histograms expressing the mean value (±SEM) of a minimum of 7 cells. *$p < 0.05$; **$p < 0.01$.

These data demonstrate that cell entry was faster and higher for NPPS than for NPPG as shown by the early boosted penetration of NPPS in macrophage-like THP-1 cells.

Mechanism of nanoparticle cell entry

Since PS-receptors expressing phagocytic THP-1 macrophages can preferentially target DPPS-filled nanoparticles, the mechanism of nanoparticle cell entry was studied in more detail. First, L-pSer was used to compete the interactions between PS (associated with nanoparticles) and PS receptors (expressed by macrophages). Cells were pretreated for 30 min with 2 mM L-pSer followed by NPPS or NPPG exposure for 0.5 or 2 h. L-pSer had no effect on NPPG or NPPS cell entry whatever the duration of exposure was (Figure 5). These data suggest that the early boost of NPPS cell loading may not be related to PS saturable receptors. Second, annexin V that displays high affinity for PS was selected to get more insight into NPPS/PS receptor interactions. Therefore, a flow cytometry-based analysis was developed to monitor nanoparticle–protein interactions in various ratio of NPPS and annexin V, and NPPG was used as a control. Consequently, NP^+ were first labelled with FITC and then filled with either DPPS or DPPG to produce FITC-labelled NPPG or NPPS, respectively. Nanoparticles were incubated for 30 min with Alexa Fluor 647-labelled annexin V before flow cytometry analysis. The nanoparticles were successively gated according to (i) size and structure (more than 450,000 events), (ii) FITC fluorescence, and (iii) Alexa Fluor 647 fluorescence. Different ratios of NPPS/annexin V and NPPG/annexin V (mass ratio: 1/0, 20/1, 4/1, and 2/1) were examined. With a 20/1 ratio, about 60% of NPPS or NPPG were associated with annexin V. With a 4/1 ratio, 95% of NPPS or NPPG

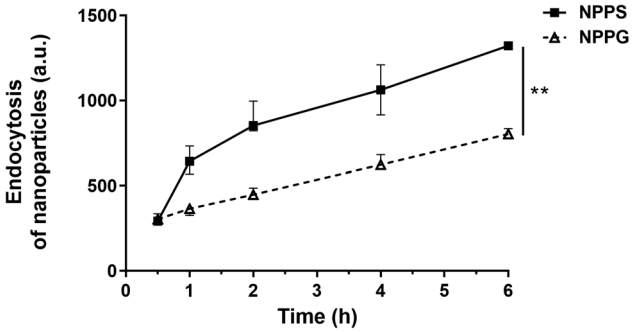

Figure 4: Endocytosis of NPPS and NPPG by macrophage-like THP-1 cells. THP-1 cells are exposed to FITC-labelled-NPPS or -NPPG for 30 min to 6 h then analysed by cytometry to determine the cellular contents of the nanoparticles. The graph represents the mean values (±SEM) of at least three experiments. **$p < 0.01$.

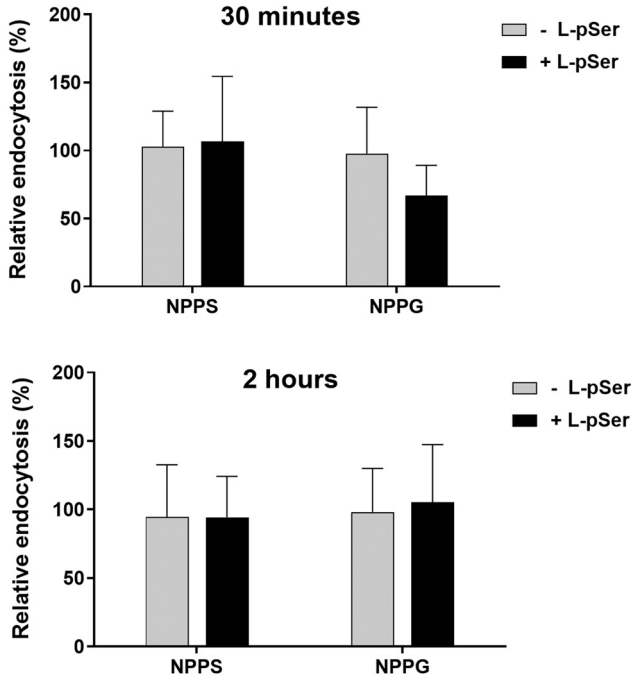

Figure 5: Inhibition of nanoparticle endocytosis by competition of PS receptors using L-pSer in macrophage-like THP-1 cells. THP-1 cells are treated for 30 min with 2 mM of L-pSer and exposed to FITC-labelled-NPPS or -NPPG for 30 min (top) or 2 h (bottom), then analysed by cytometry to determine the cellular contents of the nanoparticles. The graph represents the mean value (±SEM) of at least three experiments. No statistically significant inhibition is observed using the L-pSer.

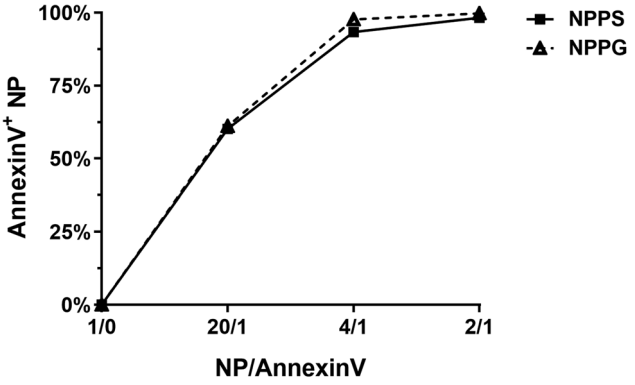

Figure 6: Accessibility of lipids associated with nanoparticles. Different mass ratios of FITC-labelled NP/annexin V-AF647 (Alexa Fluor 647) are formulated for 30 min and analysed by cytometry. Nanoparticles are first selected on their FITC fluorescence and then on the annexin V-AF647 content. No statistically significant difference is observed between NPPS and NPPG.

were associated with annexin V, while all nanoparticles interacted with annexin V with a 2/1 ratio (Figure 6). These data indicate a clear interaction between nanoparticle and annexin V which do not depend on lipid composition.

Study of protein delivery by nanoparticles

Since NPPS had better properties for macrophage-like THP-1 entry compared to NPPG, which are surprisingly not directly related to PS receptors, functional aspects of intracellular protein delivery by nanoparticles have been evaluated. For this, FITC-labelled BSA was incorporated into NPPS or NPPG, and protein association, size, and zeta potential were determined. Different mass ratios for nanoparticles/BSA (1/0, 5/1, 3/1, 1/1, 1/2, 1/3, 1/4, 1/5, and 0/1) were produced and formulations were run on non-denaturing PAGE. Under these conditions, nanoparticle-associated BSA could not migrate and gel analyses revealed only unassociated proteins. No unassociated BSA was observed for 5/1 or 3/1 ratios with NPPG or NPPS. At the ratio of 1/1, 98% of BSA was associated with NPPS and 83% with NPPG (Figure 7a and b). For further experiments, the 3/1 nanoparticles/BSA mass ratio, leading to a complete BSA association, was selected to compare the NPPS and NPPG formulations. For this ratio, BSA-NPPS and BSA-NPPG did not exhibit any significant change in size and zeta potentials compare to NPPS and NPPG (Figure 7c and d). The results demonstrate a similar association of BSA to NPPS and NPPG and suggest that BSA is integrated within the nanoparticles rather than on the surface. The capacity of NPPS and NPPG to deliver BSA into macrophage-like THP-1 cells was then investigated. Macrophage-like THP-1 cells were exposed to FITC-labelled BSA-NPPS or FITC-labelled BSA-NPPG from 0.5 to 6 h and cellular delivery of FITC-labelled BSA was analysed by cytometry. At the early time points (0.5 and 1 h), NPPS and NPPG delivered BSA in a similar manner. In contrast, from 2 to 6 h of exposure, NPPS delivered more BSA compared to NPPG (Figure 8). These data indicate that, in addition to cell entry properties, NPPS also presents enhanced capacity to deliver proteins in phagocytic cells compared to NPPG.

Characterisation of nanoparticle intracellular routes and protein processing

After nanoparticles are internalized by macrophage-like THP-1 cells, next is the intracellular routes that NPPS and NPPG follow which determine their destination within cellular compartments. As previously described, speed movements of nanoparticles were investigated in a single TIRF focal plan at the mid-cell body level. 5 min time-lapses through TIRF microscopy revealed that half of NPPS and NPPG were mobile irrespective of the duration of exposure i.e. 0.5 h or 2 h (Figure 9a). The average distance around

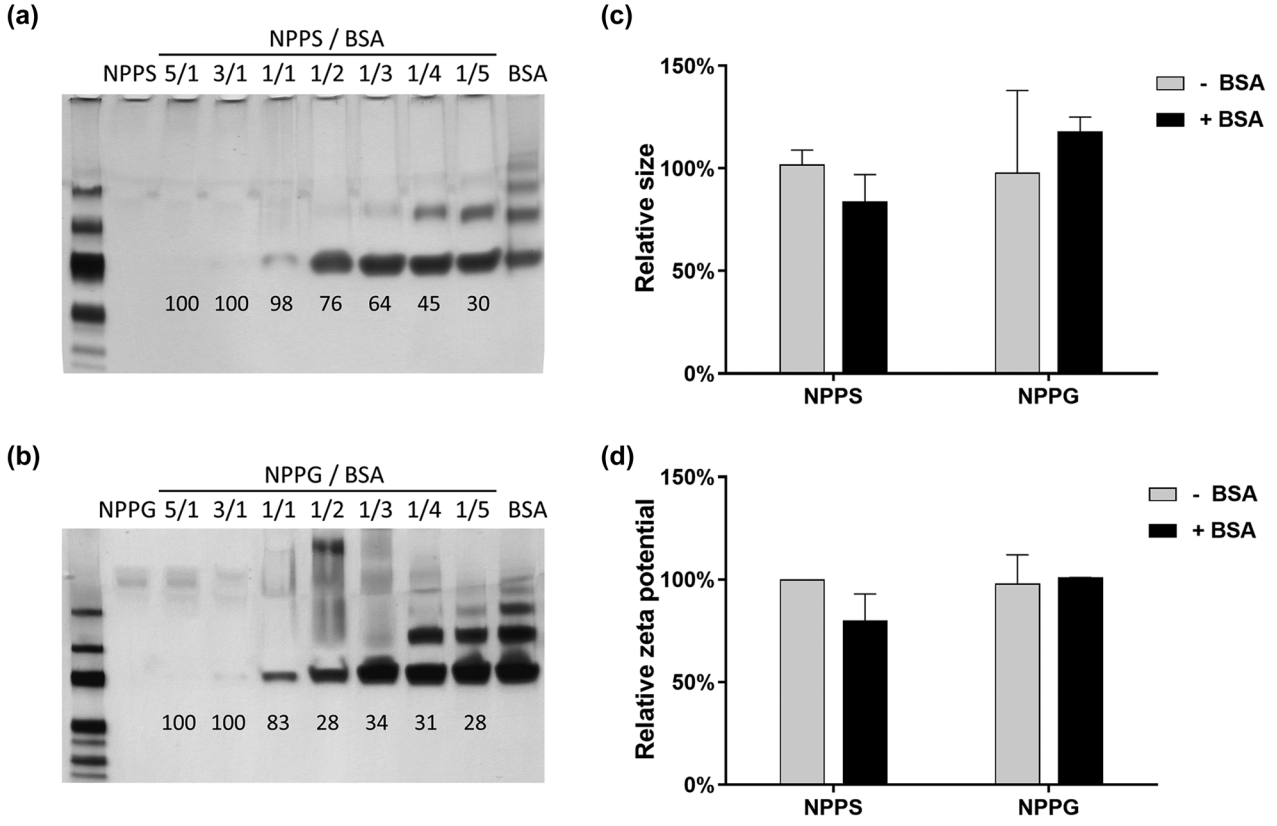

Figure 7: Association of protein by NPPS and NPPG. BSAs are used as a model protein. Different mass ratio of NPPS/BSA (a) or NPPG/BSA (b) are formulated for 30 min and run on non-denaturing polyacrylamide gel electrophoresis. Gels were imaged and quantified setting the 0% of association over the BSA input. Numbers on the gels represents the percentage of association of each formulation. The mass ratio nanoparticle/BSA: 3/1 is chosen since no free protein are detectable following silver nitrate staining of the gels. The relative size (c) and the relative zeta potential (d) of at least three formulations NPPS/BSA and NPPG/BSA (3/1) are represented on the graphs with the NPPS values set to 100%. No statistically significant difference is observed between NPPS and NPPG, with or without BSA.

3 µm covered by mobile NPPS and NPPG in 5 min was not different between particles irrespective of the duration of exposure (Figure 9b and c). Interestingly, half of NPPS and NPPG were motionless regardless of the duration of exposure i.e. 0.5 h or 2 h. Therefore, the results indicate that there is no difference between NPPS and NPPG, as well on the static as on the dynamic profiles in a 5 min time-lapse experiment. Along the intracellular routes, proteins (i.e. antigens) are processed to induce or stimulate an immune response, and the first step generally involves protein degradation by two complementary means: enzymatic and pH-decrease-dependent degradation in acid endosomes and/or lysosomes. Whether NPPS better directs proteins to vesicular degradation compared to NPPG is a main question and two approaches have been developed to test this hypothesis. First, BSA-DQ, which fluoresces when degraded by vesicular enzymes, was associated with NPPS and NPPG. Degradation of BSA-DQ in macrophage-like THP-1 cells was quantified by flow cytometry after 0.5–6 h of exposure. No difference in BSA-DQ enzymatic degradation was observed between NPPS and NPPG at any time of the experiment (Figure 10a). Second, the potential role of lipids in pH-induced vesicular protein degradation was studied (i) through a

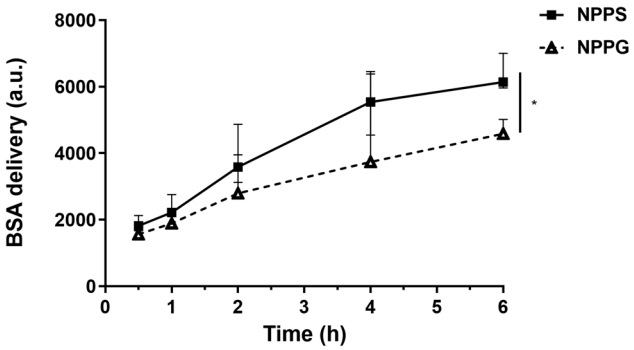

Figure 8: Protein delivery by NPPS and NPPG in macrophage-like THP-1 cells. FITC-labelled BSA is formulated (mass ratio 3/1) with NPPS or NPPG and THP-1 cells are then exposed to the formulations before cytometry analyses of the cellular BSA-FITC content. The graph represents the median fluorescence intensity (±interquartile) of three experiments. *$p < 0.05$.

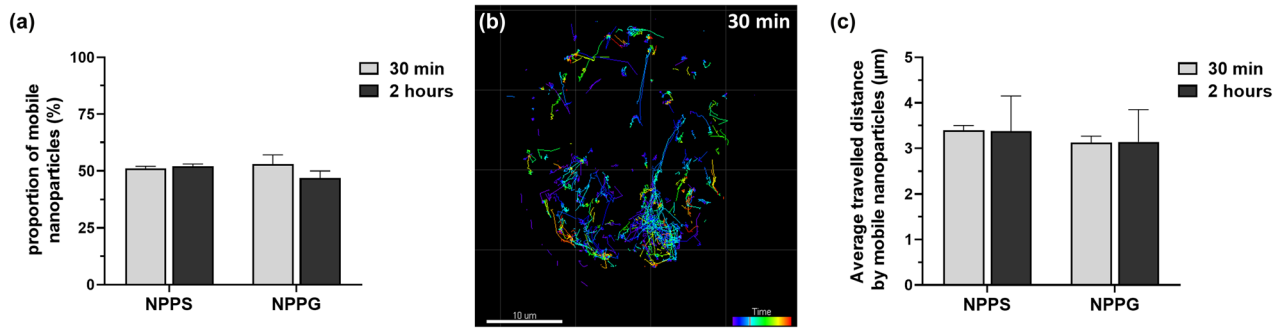

Figure 9: Characteristics of nanoparticle movement in living macrophage-like THP-1 cells through TIRF microscopy. (a) Histograms indicating the proportion of mobile nanoparticles in a single focus plane after 30 min and 2 h of exposition. No statistically significant difference is observed. (b) Illustration of NPPS tracking in a single focus plane after 30 min of exposition and using a 5 min time-lapse acquisition. Scale bar = 10 µm. Rainbow scale revealed time window of NPPS movements during time-lapse (blue, beginning; red, end). (c) Histograms indicating the average distance travelled by mobile nanoparticles within the cell. Each value represents the mean value (±SEM) of minimum five cells. No statistically significant difference is observed.

30 min pretreatment with chloroquine, which is described as an inhibitor of endosome acidification, or (ii) by using BSA-pHrodo, which is a pH-sensitive labelled protein that fluoresce at lower pH. No difference in protein degradation within chloroquine-pretreated macrophage-like THP-1 cells was observed when BSA was delivered by NPPS or NPPG (data not shown). BSA-pHrodo was formulated with NPPS and NPPG, exposed to macrophage-like THP-1 cells for 0.5–6 h and the acidification of BSA was then analysed by flow cytometry. Similarly, there was no difference in the kinetics of acidification when BSA was carried by NPPS or NPPG (Figure 10b). This suggests that, contrary to protein uptake and delivery, protein degradation through enzymatic or acidification processes was not dependent on the lipid composition of nanoparticles.

Discussion

Previous studies have underlined that (i) adjuvants and/or excipients were required for mucosal vaccines and (ii) particulate antigens such as antigens associated with nanoparticles triggered a stronger immune response than the sole antigens [28–30]. In addition, the use of vaccines assisted by cationic maltodextrin-based nanoparticles are particularly well documented [4,9,11,12,31] including comparison of NP^+ (without lipid) and NPPG benefits [5,6]. However, the role of lipid composition on the efficacy of NP^+ has never been explored so far. Here two different nanoparticles with DPPG (NPPG) and DPPS (NPPS) were developed and combined with differentiated macrophage-like THP-1 cells to investigate how PS could modulate the phagocytic cell targeting by the nanoparticles.

In the context of nasal vaccination and NP^+, lipids associated with NP^+ may have a direct impact on nanoparticle–cell interactions. Since the loading of NP^+ with different lipids has not changed the size and zeta potential characteristics (NPPS vs NPPG), this suggests that varying the lipid composition of NP^+ may generate a large family of

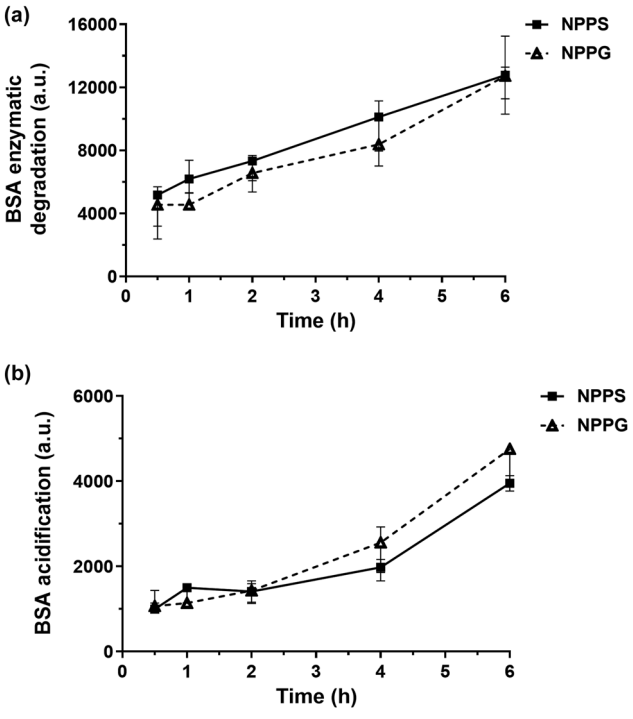

Figure 10: Characterization of nanoparticle-assisted protein degradation in macrophage-like THP-1 cells. NPPS or NPPG are formulated (mass ratio 3/1) with BSA-DQ (a) or with BSA-pH-rodo (b) to monitor the enzymatic or the pH-dependent degradation of proteins, respectively. THP-1 cells are exposed for 30 min to 6 h to the formulations and the cellular content of degraded BSA is measured by cytometry. The graphs represent the median fluorescence intensity (±interquartile) of three experiments. No statistically significant difference is observed between NPPG and NPPS.

nanocarriers with specific features and cellular interaction abilities. For example, in another procedure, a mixture of dipalmitoyl-phosphatidylcholine and glycerol was associated at the surface of NP^+, giving rise to the production of supramolecular biovectors™ [32,33]. Such a mixture could now be used to fill the NP^+ to simulate the behaviour of low-density lipoproteins [34,35].

In our working model, we hypothesized that the lipids associated with nanoparticles are of main importance and may be accessible to the surrounding environment. Moreover, previous works show that lipids are not associated with the nanoparticle's surface [6] while they modify the nanoparticle's interactions with the biological environment [5,6]. In particular, NPPG had the advantage of moving more freely than NP^+ in the artificially reconstituted mucin mixture, which is the main component of mucus [7]. This interesting NPPG property could be explained either by limited interactions between the anionic lipids and the anionic mucins [7] or by limited nanoparticle–protein interactions caused by the steric hindrance of the loaded lipids [6]. It could be of interest to describe a lipid composition that cumulate enhanced mucin permeation, enhanced antigen presenting cell targeting, and enhanced cell penetration and protein delivery. This will lead to better nasal vaccines with reduced antigen amounts.

As described, NPPGs are non-specific nanocarriers and to date, no evidence suggests a targeting of immune cells. Instead, studies about NPPG focus on nasal or respiratory epithelial cells [5,8,9]. Their role as efferocytosis-competent [36,37] or accessory immune cells [38,39] is still debated and cannot be excluded, but phagocytic cells remain the first step for antigen presentation in nasal mucosa [40]. Macrophage-like THP-1 cells that expressed PSR, TIM, and TAM receptors with affinity for PS [25] were able to perform efferocytosis. Consequently, comparative study of NPPS and NPPG were performed in these macrophage-like THP-1 cells. Confocal and TIRF microscopies provided direct evidences of nanoparticles uptake within cell body and lamellipodia of cultured macrophage-like THP-1 cells. In airway epithelial cells, NPPG and NP^+ displayed different intracellular localisation [5], indicating a role of the lipid association inside the particle and its accessibility by the environment. Here no difference in subcellular localisation could be detected for NPPG and NPPS in macrophage-like THP-1 cells. However, we showed by flow cytometry that cell entry was faster and higher for NPPS than for NPPG as suggested by the early boosted penetration of NPPS in THP-1 cells.

In cells not expressing PS-receptors, quick and massive NP^+ and NPPG endocytosis is described [5], suggesting that PS-receptors are not necessary for their cell entry, limiting the use of PS-receptor negative cells for our study. In PS-receptor expressing THP-1 cells [25], L-pSer has been described to compete with PS-dependent cell entry mechanisms, as efficiently as PS-containing liposomes [27,41]. Although a boosted early cell entry is shown for NPPS, the absence of L-pSer effect suggests that (i) the diversity of receptors with affinity to PS might not be saturated by L-pSer or (ii) other unconventional receptors might be involved. Alternatively, the early boost of NPPS cell loading may not be related to interaction between DPPS with saturable macrophage-like THP-1 cell surface receptors. Since NP^+ and NPPG have high affinity to cell surface and are able to exploit multiple endocytosis pathways in parallel [13,26], they are very efficient in cell entry [5,13] compared to widely used liposomes or poly(lactic-co-glycolic acid) nanoparticles. Therefore, PS receptors-mediated NPPS cell entry may only represent a very limited part of the overall nanoparticle uptake. Similarly, the absence of an enhanced interaction between NPPS and annexin V suggested that DPPS is not accessible by the surrounding environment. However, a competition between specific annexin V/DPPS vs non-specific annexin V/cationic maltodextrin interactions cannot be excluded since annexin V is a protein that can freely associate with the nanoparticles [6–10,31]. Although DPPS accessibility is not clear, the stimulatory effect of DPPS on cell entry and protein delivery in macrophage-like THP-1 cells is well demonstrated.

In addition to cell entry properties, intracellular protein delivery has been examined. NP^+ and derived nanoparticles have been successfully loaded with a lot of different proteins like BSA [6], ovalbumin [5,8,10], flu antigen [12,31] and even complex mixture of proteins originating from parasite lysates [9,14,15]. The simplest protein, BSA, has been used to avoid off-target mechanisms and to focus only on protein association and cellular delivery by the nanoparticles. Study with antigens inducing protective immune responses should be conducted *in vivo* to determine if NPPSs are advantageous compared to NPPG.

In our experiments, NPPSs present an enhanced capacity to deliver proteins in phagocytic cells compared to NPPG, without favouring protein degradation. The protein delivery is consistent with the increased NPPS cell entry. However, once the protein is delivered, the rate of protein degradation may be slower than that of nanoparticle uptake, constituting consequently a limiting factor that explains why there is no difference between NPPG and NPPS. Our TIRF data support that hypothesis since the proportion and travelled distance of mobile nanoparticles were similar for NPPS and NPPG. Only half of the nanoparticles were mobile, and the apparent velocity was relatively slow compared to other nanoparticles. The intracellular velocity

depends, among others, on the nanoparticle material, their interactions with the cytoskeleton, the internalisation in endocytic vesicle, the hindrance in the cell, or obviously their size. Large clusters of DNA-decorated gold nanoparticles moved at 50 nm/s in average, while the single (70 nm) exhibited an average velocity of 150 nm/s [42]. Concerning the interactions with the cytoskeleton and the endosome trafficking machinery, a velocity over 150 nm/s is described [43]. Our data showed a velocity of 10 nm/s, suggesting multiple interactions with the cellular component and an extended intracellular resident time, therefore a longer time for the carried proteins to interact with the cellular machinery. This could explain why these nanoparticles are more efficient than other conventional delivery systems [10]. In addition, while the loading of phospholipid improved the lysosome-dependent degradation of carried protein by NP^+ [5], we showed here that such a protein degradation through enzymatic or acidification processes is not dependent on the lipid composition. Taken together these data suggest that when nanoparticles entered cells, they waited for being processed or addressed to organelles or exocytosis. However, nanocarriers with enhanced delivery properties through the mucosal barrier may ultimately reduce the initial amount of required antigens to trigger the immune response [44].

In conclusion, macrophage-like THP-1 cells can be considered as a model to investigate the mechanisms of NP^+-assisted immune response in the context of nasal vaccination. The nanoparticle can be filled with lipids whose composition drives properties. In particular, cell entry and protein delivery were higher for NPPS than for NPPG. Since cell loading may not be related to PS receptors, this study highlighted a mechanism unrevealed so far. Within macrophage-like THP-1 cells, half of the nanoparticles were mobile and protein degradation through enzymatic or acidification processes was not dependent on the nanoparticle-associated lipid composition. Nanoparticles with enhanced cell entry and delivery properties may reduce the quantity of antigens and associated cost to trigger an immune response. Further *in vivo* nanoparticle-assisted vaccine studies are required to fully settle the strategy.

Acknowledgements: We would like to thank the Flow Core Facility of BioImaging Center Lille – UAR2014-US41-PLBS – (F-59000 Lille, France) for the expert technical assistance.

Funding information: No specific funding was received for this study. R.C., C.B., and L.D. were supported by the University of Lille, INSERM, and CHU Lille. PRIMACEN was supported by the University of Rouen Normandy, Inserm, IRIB, Région Normandie (RIN plate-forme "7D microscopy"), the European Regional Development Fund (ERDF "7D Microscopy"), and the GIS IBiSA.

Authors contributions: Conceptualisation: R.C., L.D., L.G., and M.T.; methodology: C.B., R.C., and L.G.; validation: C.B., M.B., A.L., and D.S.; formal analysis: C.B.; investigation: C.B., M.B., A.L., and D.S. writing – original draft: R.C., L.G., and M.T.; writing – review and editing: R.C., L.D., and L.G.: visualization: C.B., M.B., A.L., D.S., R.C., and L.G.; supervision: R.C., L.D., and L.G.; project administration: R.C., L.D., and L.G.; funding acquisition: L.D.

Conflict of interest: Authors state no conflict of interest.

Data availability statement: The datasets generated during and/or analysed during the current study are available from the corresponding author on reasonable request.

References

[1] Meenakshi S, Kumar VU, Dhingra S, Murti K. Nasal vaccine as a booster shot: A viable solution to restrict pandemic? Clin Exp Vaccine Res. 2022;11(2):184–92.

[2] Bernocchi B, Carpentier R, Betbeder D. Nasal nanovaccines. Int J Pharm. 2017;530(1–2):128–38.

[3] Huang J, Ding Y, Yao J, Zhang M, Zhang Y, Xie Z, et al. Nasal nanovaccines for SARS-CoV-2 to address COVID-19. Vaccines (Basel). 2022;10(3):405.

[4] Kravtzoff R, Betbeder D, Davrinche C, Vaz Santiago J, Lule J. Use of hydrophilic particles associated with antigens for preparing vaccine compositions. Patent WO/2002/034239; 2002.

[5] Dombu C, Carpentier R, Betbeder D. Influence of surface charge and inner composition of nanoparticles on intracellular delivery of proteins in airway epithelial cells. Biomaterials. 2012;33(35):9117–26.

[6] Paillard A, Passirani C, Saulnier P, Kroubi M, Garcion E, Benoit JP, et al. Positively-charged, porous, polysaccharide nanoparticles loaded with anionic molecules behave as 'stealth' cationic nanocarriers. Pharm Res. 2010;27(1):126–33.

[7] Fasquelle F, Carpentier R, Demouveaux B, Desseyn JL, Betbeder D. Importance of the phospholipid core for mucin hydrogel penetration and mucosal cell uptake of maltodextrin nanoparticles. ACS Appl Bio Mater. 2020;3(9):5741–9.

[8] Bernocchi B, Carpentier R, Lantier I, Ducournau C, Dimier-Poisson I, Betbeder D. Mechanisms allowing protein delivery in nasal mucosa using NPL nanoparticles. J Controlled Rel. 2016;232:42–50.

[9] Dimier-Poisson I, Carpentier R, N'Guyen TT, Dahmani F, Ducournau C, Betbeder D. Porous nanoparticles as delivery system of complex antigens for an effective vaccine against acute and chronic Toxoplasma gondii infection. Biomaterials. 2015;50:164–75.

[10] Le MQ, Carpentier R, Lantier I, Ducournau C, Fasquelle F, Dimier-Poisson I, et al. Protein delivery by porous cationic maltodextrin-based nanoparticles into nasal mucosal cells: Comparison with cationic or anionic nanoparticles. Int J Pharm X. 2019;1:100001.

[11] De Miguel I, Imbertie L, Betbeder D, Lescure F, Kravtzoff R. Amphilic and ionic polymer matrixes and derivatives thereof. Patent WO/2001/051090, 2001.
[12] Le MQ, Ye L, Bernasconi V, Carpentier R, Fasquelle F, Lycke N, et al. Prevention of influenza virus infection and transmission by intranasal administration of a porous maltodextrin nanoparticle-formulated vaccine. Int J Pharm. 2020;582:119348.
[13] Le MQ, Carpentier R, Lantier I, Ducournau C, Dimier-Poisson I, Betbeder D. Residence time and uptake of porous and cationic maltodextrin-based nanoparticles in the nasal mucosa: Comparison with anionic and cationic nanoparticles. Int J Pharm. 2018;550(1–2):316–24.
[14] Ducournau C, Nguyen TT, Carpentier R, Lantier I, Germon S, Precausta F, et al. Synthetic parasites: A successful mucosal nanoparticle vaccine against toxoplasma congenital infection in mice. Future Microbiol. 2017;12:393–405.
[15] Ducournau C, Moire N, Carpentier R, Cantin P, Herkt C, Lantier I, et al. Effective nanoparticle-based nasal vaccine against latent and congenital toxoplasmosis in sheep. Front Immunol. 2020;11:2183.
[16] Boada-Romero E, Martinez J, Heckmann BL, Green DR. The clearance of dead cells by efferocytosis. Nat Rev Mol Cell Biol. 2020;21(7):398–414.
[17] Kuchroo VK, Umetsu DT, DeKruyff RH, Freeman GJ. The TIM gene family: Emerging roles in immunity and disease. Nat Rev Immunol. 2003;3(6):454–62.
[18] DeKruyff RH, Bu X, Ballesteros A, Santiago C, Chim YL, Lee HH, et al. T cell/transmembrane, Ig, and mucin-3 allelic variants differentially recognize phosphatidylserine and mediate phagocytosis of apoptotic cells. J Immunol. 2010;184(4):1918–30.
[19] Bonnardel J, Da Silva C, Henri S, Tamoutounour S, Chasson L, Montanana-Sanchis F, et al. Innate and adaptive immune functions of peyer's patch monocyte-derived cells. Cell Rep. 2015;11(5):770–84.
[20] Nagata S. Apoptosis and clearance of apoptotic cells. Annu Rev Immunol. 2018;36:489–517.
[21] Oliveira LG, Peron JPS. Viral receptors for flaviviruses: Not only gatekeepers. J Leukoc Biol. 2019;106(3):695–701.
[22] Chua BA, Ngo JA, Situ K, Morizono K. Roles of phosphatidylserine exposed on the viral envelope and cell membrane in HIV-1 replication. Cell Commun Signal. 2019;17(1):132.
[23] Birge RB, Boeltz S, Kumar S, Carlson J, Wanderley J, Calianese D, et al. Phosphatidylserine is a global immunosuppressive signal in efferocytosis, infectious disease, and cancer. Cell Death Differ. 2016;23(6):962–78.
[24] Wanderley JLM, DaMatta RA, Barcinski MA. Apoptotic mimicry as a strategy for the establishment of parasitic infections: Parasite- and host-derived phosphatidylserine as key molecule. Cell Commun Signal. 2020;18(1):10.
[25] Forrester MA, Wassall HJ, Hall LS, Cao H, Wilson HM, Barker RN, et al. Similarities and differences in surface receptor expression by THP-1 monocytes and differentiated macrophages polarized using seven different conditioning regimens. Cell Immunol. 2018;332:58–76.
[26] Salah N, Dubuquoy L, Carpentier R, Betbeder D. Starch nanoparticles improve curcumin-induced production of anti-inflammatory cytokines in intestinal epithelial cells. Int J Pharm X. 2022;4:100114.
[27] Kurosaka K, Watanabe N, Kobayashi Y. Production of proinflammatory cytokines by phorbol myristate acetate-treated THP-1 cells and monocyte-derived macrophages after phagocytosis of apoptotic CTLL-2 cells. J Immunol. 1998;161(11):6245–9.
[28] Hagenaars N, Mastrobattista E, Glansbeek H, Heldens J, van den Bosch H, Schijns V, et al. Head-to-head comparison of four nonadjuvanted inactivated cell culture-derived influenza vaccines: Effect of composition, spatial organization and immunization route on the immunogenicity in a murine challenge model. Vaccine. 2008;26(51):6555–63.
[29] Vanloubbeeck Y, Pichyangkul S, Bayat B, Yongvanitchit K, Bennett JW, Sattabongkot J, et al. Comparison of the immune responses induced by soluble and particulate plasmodium vivax circumsporozoite vaccine candidates formulated in AS01 in rhesus macaques. Vaccine. 2013;31(52):6216–24.
[30] Deng L, Mohan T, Chang TZ, Gonzalez GX, Wang Y, Kwon YM, et al. Double-layered protein nanoparticles induce broad protection against divergent influenza A viruses. Nat Commun. 2018;9(1):359.
[31] Bernasconi V, Bernocchi B, Ye L, Le MQ, Omokanye A, Carpentier R, et al. Porous nanoparticles with self-adjuvanting M2e-fusion protein and recombinant hemagglutinin provide strong and broadly protective immunity against influenza virus infections. Front Immunol. 2018;9:2060.
[32] Castignolles N, Morgeaux S, Gontier-Jallet C, Samain D, Betbeder D, Perrin P. A new family of carriers (biovectors) enhances the immunogenicity of rabies antigens. Vaccine. 1996;14(14):1353–60.
[33] von Hoegen P. Synthetic biomimetic supra molecular biovector (SMBV) particles for nasal vaccine delivery. Adv Drug Deliv Rev. 2001;51(1-3):113–25.
[34] De Miguel I, Ioualalen K, Bonnefous M, Peyrot M, Nguyen F, Cervilla M, et al. Synthesis and characterization of supramolecular biovector (SMBV) specifically designed for the entrapment of ionic molecules. Biochim Biophys Acta. 1995;1237(1):49–58.
[35] Peyrot M, Sautereau AM, Rabanel JM, Nguyen F, Tocanne JF, Samain D. Supramolecular biovectors (SMBV): A new family of nanoparticulate drug delivery systems. Synthesis and structural characterization. Int J Pharm. 1994;102(1):25–33.
[36] Davies SP, Reynolds GM, Stamataki Z. Clearance of apoptotic cells by tissue epithelia: A putative role for hepatocytes in liver efferocytosis. Front Immunol. 2018;9:44.
[37] Seeberg JC, Loibl M, Moser F, Schwegler M, Buttner-Herold M, Daniel C, et al. Non-professional phagocytosis: A general feature of normal tissue cells. Sci Rep. 2019;9(1):11875.
[38] Salik E, Tyorkin M, Mohan S, George I, Becker K, Oei E, et al. Antigen trafficking and accessory cell function in respiratory epithelial cells. Am J Respir Cell Mol Biol. 1999;21(3):365–79.
[39] McDougall CM, Blaylock MG, Douglas JG, Brooker RJ, Helms PJ, Walsh GM. Nasal epithelial cells as surrogates for bronchial epithelial cells in airway inflammation studies. Am J Respir Cell Mol Biol. 2008;39(5):560–8.
[40] Jahnsen FL, Gran E, Haye R, Brandtzaeg P. Human nasal mucosa contains antigen-presenting cells of strikingly different functional phenotypes. Am J Respir Cell Mol Biol. 2004;30(1):31–7.
[41] Fadok VA, Bratton DL, Rose DM, Pearson A, Ezekewitz RA, Henson PM. A receptor for phosphatidylserine-specific clearance of apoptotic cells. Nature. 2000;405(6782):85–90.
[42] Liu M, Li Q, Liang L, Li J, Wang K, Li J, et al. Real-time visualization of clustering and intracellular transport of gold nanoparticles by correlative imaging. Nat Commun. 2017;8:15646.
[43] Toshima JY, Toshima J, Kaksonen M, Martin AC, King DS, Drubin DG. Spatial dynamics of receptor-mediated endocytic trafficking in budding yeast revealed by using fluorescent alpha-factor derivatives. Proc Natl Acad Sci U S A. 2006;103(15):5793–8.
[44] Mao L, Chen Z, Wang Y, Chen C. Design and application of nanoparticles as vaccine adjuvants against human corona virus infection. J Inorg Biochem. 2021;219:111454.